JOURNAL OF THE KOREAN ASTRONOMICAL SOCIETY
40: 179 ~ 182, 2007

# GAS-DYNAMICAL FRICTION OF A PERTURBER MOVING ON A CIRCULAR ORBIT

HYOSUN KIM[1] AND WOONG-TAE KIM[1]
[1] Department of Physics and Astronomy, Seoul National University, Seoul 151-742, Korea
*E-mail: hkim@astro.snu.ac.kr, wkim@astro.snu.ac.kr*
*(Received December 4, 2007; Accepted December 13, 2007)*

## ABSTRACT

Dynamical friction plays an important role in reducing angular momenta of objects in orbital motions. While astronomical objects usually follow curvilinear orbits, most previous studies focused on the linear-trajectory cases. Here, we present the gravitational wake due to, and dynamical friction on, a perturber moving on a circular orbit in a uniform gaseous medium using a semi-analytic method. The circular orbit causes the density wakes to bend along the orbit into asymmetric configurations, resulting in the drag forces in both opposite (azimuthal) and lateral (radial) directions to the perturber motion, although the latter does not contribute to the orbital decay much. For a subsonic perturber, the bending of a wake is only modest and the resulting drag force in the opposite direction is remarkably similar to the linear-trajectory counterpart. On the other hand, a supersonic perturber is able to overtake its own wake, possibly multiple times, creating a high-density trailing tail. Despite the dramatic changes in the wake morphologies, the azimuthal drag force is in surprisingly good agreement with the formulae of Ostriker for the linear-trajectory cases, provided $V_p t = 2R_p$, where $V_p$ and $R_p$ are the velocity and orbital radius of the perturber, respectively.

*Key words :* hydrodynamics — ISM: general — shock waves

## I. INTRODUCTION

A massive object in orbital motion interacts with a background medium through gravity, forms a density wake, subsequently experiences a momentum loss due to its gravitational interaction with the wake, and decays toward the center of the orbit, the whole sequence of which is referred to as dynamical friction. This mechanism was first discussed in detail by Chandrasekhar (1943) who derived the classical formula for the drag force in a collisionless background, and has since been applied to a large number of astronomical systems (e.g., Binney & Tremaine 1987). Comparatively, dynamical friction in a gaseous background was less well recognized until Ostriker (1999) who recently derived the analytic expressions for the density wake and drag forces for a perturber in a uniform gaseous medium. She found that a supersonic perturbers develops a cone-like density wake, while a subsonic motion produces an ellipsoidal wake. She also found that the gaseous drag is more efficient than the collisionless drag at the Mach number $\mathcal{M} \sim 1$ and non-vanishing even in the subsonic cases (see also Dokuchaev 1964; Ruderman & Spiegel 1971; Rephaeli & Salpeter 1980).

Gas-dynamical friction can be important in various astronomical systems including the merging of massive black holes in galactic nuclei (Escala et al. 2004, 2005; Dotti et al. 2006), orbital decay of compact objects (Narayan 2000; Karas & Šubr 2001) and associated viscous heating (Chang 2001) in accretion disks, and the heating of an intracluster medium by supersonically moving galaxies in clusters (El-Zant et al. 2004; Kim et al. 2005). While these authors applied the results of Ostriker (1999) in their analyses, perturbers in real astronomical situations are more likely to follow curvilinear orbits rather than linear trajectories. In this presentation, we review our recent work that extends the finite-time, linear-perturbation analysis of Ostriker (1999) to study dynamical friction of a circular-orbit perturber. Our main objective is to find how the wake structures and the associated drag forces change as a orbital shape of the perturber varies. The reader is referred to Kim & Kim (2007) for more comprehensive derivations and discussions.

*Corresponding Author*: H. Kim

## II. DENSITY WAKE

We begin with the basic equations of hydrodynamics for an inviscid, adiabatic gas without self-gravity and magnetic fields. After linearizing the continuity and momentum equations and combining the resulting equations, we obtain

$$\nabla^2 \alpha - \frac{1}{c_s^2}\frac{\partial^2 \alpha}{\partial t^2} = -\frac{4\pi G}{c_s^2}\rho_{\rm ext}(\boldsymbol{x}, t), \qquad (1)$$

where $\alpha(\boldsymbol{x}, t) \equiv \rho/\rho_0 - 1$ is the density enhancement of the gas which is initially uniform ($\rho[\boldsymbol{x}, t = 0] = \rho_0$), $c_s$ is an adiabatic speed of sound, and $\rho_{\rm ext}$ represents the mass density of the perturber. For a perturber of mass $M_p$ that is moving with a constant linear velocity $V_p$

on a circular orbit of radius $R_p$, $\rho_{\rm ext}(\boldsymbol{x},t) = M_p\,\delta(R - R_p)\,\delta[R_p(\varphi - \Omega t)]\,\delta(z)\,\mathcal{H}(t)$ where $\Omega \equiv V_p/R_p$ is the constant angular velocity and $\mathcal{H}(t)$ is a Heaviside step function. Using the retarded Green functions, equation (1) is then reduced to

$$\alpha(\boldsymbol{x},t) = \frac{GM_p}{c_{\rm s}^2 R_p}\,\mathcal{D}(\boldsymbol{x},t), \tag{2}$$

where $\mathcal{D}(\boldsymbol{x},t)$ is the dimensionless perturbed density defined by

$$\mathcal{D}(\boldsymbol{x},t) = \sum_{w_i} \frac{\mathcal{M}}{|w_i + s - \mathcal{M}^2(R/R_p)\sin w_i|}\,\mathcal{H}\!\left(\frac{w_i+\varphi}{\Omega}\right). \tag{3}$$

In equation (3), $w \equiv \varphi' - \varphi$ and $s \equiv \varphi - \Omega t$ are the angular distances of the perturber when the perturbations were launched and at the present time, respectively, relative to the position of interest in the orbital plane, and $\mathcal{M} \equiv V_p/c_{\rm s}$ is the Mach number of the perturber, and $w_i$ represents all possible roots of $w$ that satisfy the condition

$$\frac{\mathcal{M}}{R_p}\,(R^2 + z^2 + R_p^2 - 2R_pR\cos w)^{1/2} = -(w_i + s), \tag{4}$$

for fixed values of $R$, $z$, and $s$.

In order to find the perturbed density distribution $\mathcal{D}(\boldsymbol{x},t)$, we solve equations (3) and (4) numerically. Figure 1 shows the density wakes for $\mathcal{M} = 0.6$, 1.0, 3.2, and 6.0. For subsonic perturbers, the circular orbits cause the bending of density wakes that would otherwise remain axisymmetric. As Mach number increases, the wake bends more and more, developing a long trailing tail. Perturbers of a supersonic speed introduce shocks that produce sharp edges in the wakes. Furthermore, a supersonic perturber on a closed orbit is able to enter the backside of its wake which was created about an orbital period ago, making the wakes much more complicated than those in linear-trajectory cases. This is overall in good agreement with the results of numerical simulations by by Sánchez-Salcedo & Brandenburg (2001) and Escala (2004). Figure 2 shows how the a perturber overtakes its density wake in the case of $\mathcal{M} = 5.0$. It is apparent that at $t \approx 1.8$ the perturber (or the head of the wake) begin to penetrate the one side of the wake tail and create a new narrow tail of high density.

A tail thickens as the Mach number increases from unity. At $\mathcal{M} \approx 4.6$, a fat tail eventually fills the whole area except near the center, enabling its inner edge to contact the neighboring outer edge. As $\mathcal{M}$ increases further, the tail overlaps itself, producing a new high-density, thin tail. The new tail again becomes thicker along Mach number until reaching $\mathcal{M} \approx 7.8$ at which another overlapping event occurs. Physically, the self-overlapping of the tail implies that the overlapping zone receives an additional perturbations from the perturber.

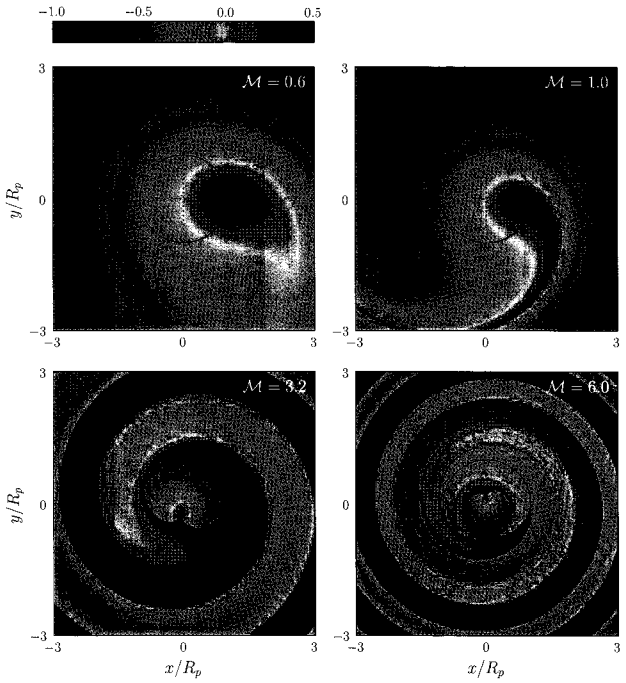


**Fig. 1.**— Steady-state distributions of the perturbed density $\mathcal{D}$ in logarithmic color scale on the orbital plane for $\mathcal{M} = 0.6$ (*top left*), 1.0 (*top right*), 3.2 (*bottom left*), and 6.0 (*bottom right*). In each frame, the perturber rotating in the counterclockwise direction is located at $(x, y) = (R_p, 0)$, and moves on the circular orbit marked by the black circle with radius $R_p$.

## III. GRAVITATIONAL FORCE

Once the distribution of a density wake is found, the drag forces on the perturber can be evaluated by simply integrating the contributions from each mass element constituting the wake. Since the wake is symmetric relative to the orbital plane, the drag force is zero in the vertical direction. We decompose the non-vanishing part into two components:

$$\boldsymbol{F}_{\rm DF} = -\frac{4\pi\rho_0(GM_p)^2}{V_p^2}\left(\mathcal{I}_R\hat{\boldsymbol{R}} + \mathcal{I}_\varphi\hat{\boldsymbol{\varphi}}\right), \tag{5}$$

where $\mathcal{I}_R$ and $I_\varphi$ are the dimensionless forces in the radial (central) and azimuthal (backward) directions. Figure 3 plots $\mathcal{I}_R$ (dashed line) and $I_\varphi$ (solid line) as function of the Mach number of the perturber. Note that both peak at $\mathcal{M} \sim 1.2 - 1.4$, similarly to the drag forces in the linear-trajectory cases. While $\mathcal{I}_R$ falls steeply and is smaller than $\mathcal{I}_\varphi$ as $\mathcal{M}$ decreases from unity, it exceeds $\mathcal{I}_\varphi$ for $\mathcal{M} \gtrsim 2.2$. However, we find that $\mathcal{I}_R$ plays a minor role in the orbital decay of a perturber. This is because the drag force in the radial direction is much smaller than the centrifugal force arising from the perturber rotation, so that $\mathcal{I}_R$ makes only a small change in the total radial force.

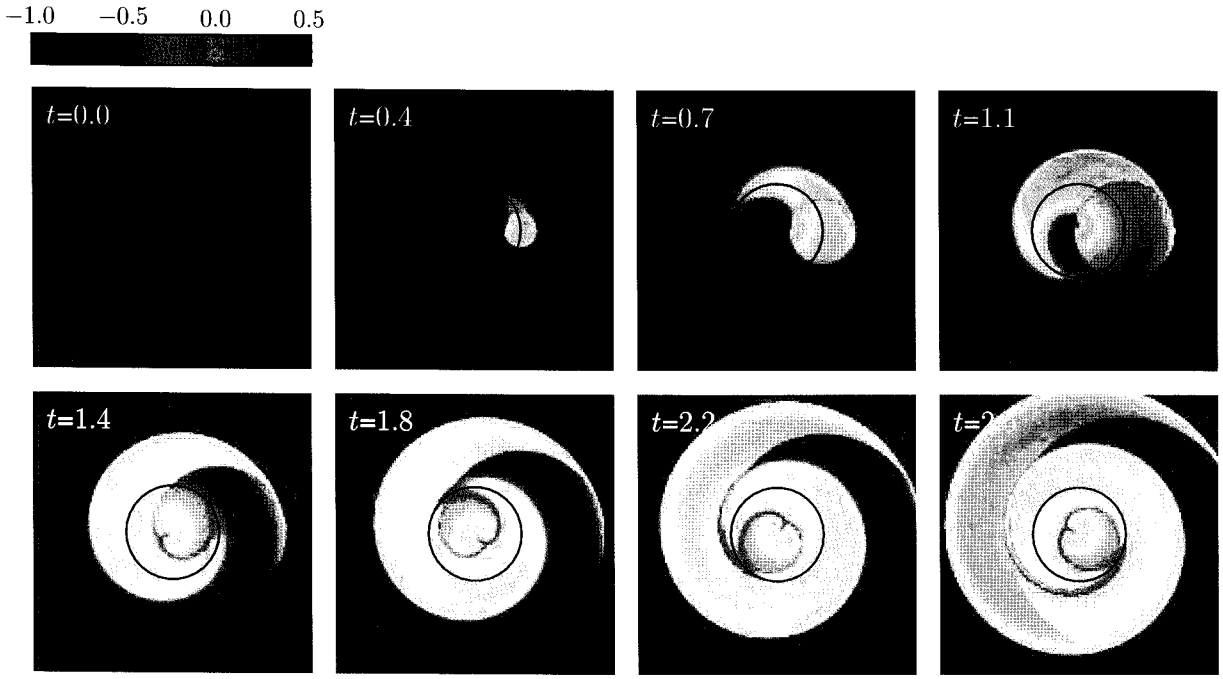


**Fig. 2.**— Temporal evolution of the density wake for $\mathcal{M} = 5.0$. The perturber orbits along the black circle in the counterclockwise direction. Time is in units of $R_p/c_s$. Color bar labels $\log \mathcal{D}$.

Local bumps seen in $\mathcal{I}_R$ at $\mathcal{M} \approx 4.6$ and 7.8 reflect the self-overlapping of the wake tail, as discussed in the previous section.

Figure 3 also plots as a dotted curve the results of Ostriker (1999) with $V_p t = 2R_p$ for linear-trajectory cases, which are in good agreement with the azimuthal drag force $\mathcal{I}_\varphi$. It is remarkable that the wakes with quite different shapes give rise to drag forces that are similar to each other. The agreement is excellent for the subsonic motions, which implies that except for bending, the wake structure created by a subsonic circular-orbit perturber is not significantly different from the linear-trajectory counterpart.

The drag force suffered by a linear-trajectory perturber depends on $V_p t$, the linear distance traveled by it, which will be infinitely large if the steady state is to be attained (i.e., $t \to \infty$). In usual applications of dynamical friction, it is customary to take $V_p t$ equal to the radial extent $R_{\rm sys}$ of a system in consideration through which sonic perturbations propagate. However, our results suggest that when a perturber moves one a near-circular orbit with radius $R_p$, $2R_p$ is a better approximation to $V_p t$ if one is to apply the linear-trajectory drag force formula with the same Mach number. Since $R_{\rm sys}$ is larger than $2R_p$ in most relevant situations, the force formula for linear-trajectory cases with $R_{\rm sys}$ would overestimate the circular-orbit drag force. Our suggestion of using $2R_p = V_p t$ is consistent with the results of hydrodynamic simulations by Sánchez-Salcedo & Brandenburg (2001) who found that the characteristic scale varying proportionally to the orbital radius gives more accurate estimates to the decay timescales. In fact, a circular orbit naturally introduces a characteristic length scale $R_p$, which is unlike in straight-line trajectory cases.

## IV. SUMMARY

Using a semi-analytic method, we have investigated the spatial structure and shape of a density wake induced by a massive perturber moving on a circular-orbit in a uniform gaseous medium, and the drag force applied to the perturber gravitationally by the wake. We find that a density wake of a subsonic perturber is a simply curved version of what is produced by the linear-trajectory counterpart, making the resulting drag forces almost independent of the shape of the perturber orbit. On the other hand, a supersonic perturber allows sonic perturbations to overlap at spatially-localized regions, eventually turning out as a pronounced tail in a spiral shape. Although this may suggest that the drag forces for circular-orbit supersonic perturbers are different from those in Ostriker (1999) for linear-trajectory cases, it is found that the latter approximates the former remarkably well as long as $V_p t = 2R_p$ is taken in the Ostriker's formula.

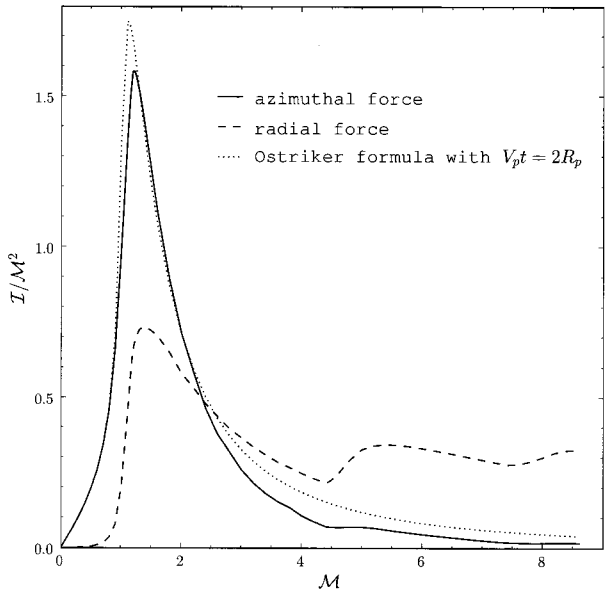


**Fig. 3.**— Steady-state gravitational drag forces for a circular-orbit perturber in a gaseous medium as functions of Mach number $\mathcal{M}$. The solid and dashed curves plot the results of our semi-analytic calculation for the drag forces in the azimuthal and radial directions, respectively. The dotted line corresponds to the force formula with $V_p t = 2R_p$ in Ostriker (1999) for the case of linear-trajectory perturbers, which is in remarkably good agreement with the azimuthal drag force for circular-orbit perturbers. For all the curves, $r_{\rm min}/R_p = 0.1$ is taken.

## REFERENCES

Binney, J., & Tremaine, S. 1987, Galactic Dynamics (Princeton: Princeton Univ. Press)

Chandrasekhar, S. 1943, Dynamical Friction. I. General Considerations: the Coefficient of Dynamical Friction, ApJ, 97, 255

Chang, H.-Y. 2001, Cooling a Hot Disk around a Supermassive Black Hole by a Star, ApJ, 551, L159

Dokuchaev, V. P. 1964, Emission of Magnetoacoustic Waves in the Motion of Stars in Cosmic Space, Soviet Astron, 8, 23

Dotti, M., Colpi, M., & Haardt, F. 2006, Laser Interferometer Space Antenna double black holes: dynamics in gaseous nuclear discs, MNRAS, 367, 103

El-Zant, A. A., Kim, W.-T., & Kamionkowski, M. 2004, Dynamical-friction galaxy-gas coupling and cluster cooling flows, MNRAS, 354, 169

Escala, A., Larson, R. B., Coppi, P. S., & Mardones, D. 2004, The Role of Gas in the Merging of Massive Black Holes in Galactic Nuclei. I. Black Hole Merging in a Spherical Gas Cloud, ApJ, 607, 765

Escala, A., Larson, R. B., Coppi, P. S., & Mardones, D. 2005, The Role of Gas in the Merging of Massive Black Holes in Galactic Nuclei. II. Black Hole Merging in a Nuclear Gas Disk, ApJ, 630, 152

Karas, V., Šubr, L. 2001, Orbital decay of satellites crossing an accretion disc, A&A, 376, 686

Kim, W.-T., El-Zant, A. A., & Kamionkowski, M. 2005, Dynamical Friction and Cooling Flows in Galaxy Clusters, ApJ, 632, 157

Kim, H., & Kim, W.-T. 2007, Dynamical Friction of a Circular-Orbit Perturber in a Gaseous Medium, ApJ, 665, 432

Narayan, R. 2000, Hydrodynamic Drag on a Compact Star Orbiting a Supermassive Black Hole, ApJ, 536, 663

Ostriker, E. C. 1999, Dynamical Friction in a Gaseous Medium, ApJ, 513, 252 (O99)

Rephaeli, Y., & Salpeter, E. E. 1980, Flow past a massive object and the gravitational drag, ApJ, 240, 20

Ruderman, M. A., & Spiegel, E. A. 1971, Galactic Wakes, ApJ, 165, 1

Sánchez-Salcedo, F. J., & Brandenburg, A. 1999, Deceleration by Dynamical Friction in a Gaseous Medium, ApJ, 522, L35

Sánchez-Salcedo, F. J., & Brandenburg, A. 2001, Dynamical friction of bodies orbiting in a gaseous sphere, MNRAS, 322, 67